Solar Energy 263 (2023) 111929

Contents lists available at ScienceDirect

Solar Energy

journal homepage: www.elsevier.com/locate/solener

Modeling of highly efficient CNGS based kesterite solar cell: A DFT study along with SCAPS-1D analysis

N. El Ouarie [a,b], J. El Hamdaoui [a,b], G.S. Sahoo [c], K.G. Rodriguez-Osorio [d], M. Courel [d], M. Zazoui [e], L.M. Pérez [f,*], D. Laroze [g], E. Feddi [a,h]

[a] Group of Optoelectronic of Semiconductors and Nanomaterials, ENSAM, Mohammed V University in Rabat, Morocco
[b] Laboratory of Condensed Matter and Interdisciplinary Sciences (LaMCScI), Faculty of Sciences Rabat, Mohammed V University in Rabat, Morocco
[c] School of Electronics Engineering (SENSE), Vellore Institute of Technology, Vandalur-Kellambakkam Road, Chennai, Tamil Nadu 600127, India
[d] Centro Universitario de los Valles, Universidad de Guadalajara, Carretera Guadalajara-Ameca, 46600, Ameca, Jalisco, Mexico
[e] Laboratory of Physics of Condensed Matter and Renewable Energy, Faculty of Sciences and Technology, Hassan II University of Casablanca, 146 Mohammedia, Morocco
[f] Departamento de Física, FACI, Universidad de Tarapacá, Casilla 7D, Arica, Chile
[g] Instituto de Alta Investigación, Universidad de Tarapacá, Casilla 7D, Arica, Chile
[h] Institute of Applied Physics, Mohammed VI Polytechnic University, Lot 660, Hay Moulay Rachid Ben Guerir, 43150, Morocco

ARTICLE INFO

Keywords:
Kesterite
Solar cell
Defect density
Absorption coefficient
CNGS

ABSTRACT

The electronic and optical properties of Cu_2NiGeS_4 (CNGS) are examined using the first-principle DFT calculations. A unique mBJ + U potential method is used for the band gap energy calculation of CNGS. With a remarkably high absorption coefficient (10^4 cm^{-1}), CNGS has become a promising candidate for photovoltaic applications. SCAPS-1D tool is used to simulate a thin-film solar cell with a $Mo/MoS_2/Cu_2NiGeS_4$ (CNGS)/CdS/ZnO/ZnO:Al structure. The impact of various factors, such as layer thickness, donor and acceptor concentrations, and defect density on the CNGS layer was explored. This study also explores the combination of suitable buffer layers (such as CdS, ZnS, and their alloy $Cd_{1-x}Zn_xS$), along with different doping concentrations and thicknesses, to be used as suitable buffer layers in the CNGS solar cell. The simulation outcomes suggest that the optimal thickness for the absorption layer in CNGS solar cells is between 2000 and 2400 nm, while the ideal thickness for MoS_2 is 100 nm. The buffer layer should be between 20 and 50 nm. Keeping the defect density of CNGS below 10^{14} cm^{-3} is crucial for high efficiency. The optimized results yield an efficiency conversion rate of 20.05%, a 66.77% fill factor, a short-circuit current of 29.67 mA/cm^2 and an open-circuit voltage of 0.983 V.

1. Introduction

The demand for cost-effective and environmentally friendly renewable energy sources has become crucial in the current era. Photovoltaic systems offer a solution to fulfill this energy demand by providing high energy conversion efficiency and extended material lifespan [1]. By embracing the adoption of photovoltaic systems, we not only address the need for sustainable energy sources but also actively contribute to the global transition towards carbon neutrality and the mitigation of global warming, as outlined in the Paris Agreement [2]. In the pursuit of progress in thin-film technology, compound semiconductor materials such as CdTe, CdSe, CIGS ($CuInGaSe_2$), GaAs, GaN, and perovskite, as well as their composites have emerged as a highly promising substitute for conventional silicon-based technology. However, certain drawbacks hinder their widespread adoption. For instance: CdTe is associated with the toxic element cadmium (Cd), CIGS contains expensive and rareearth elements like gallium (Ga) and indium (In) while perovskite materials face stability issues limiting their commercial viability on a large scale [3]. In order to address these challenges, it is essential to explore new materials that possess a combination of key properties such as non-toxicity, abundant availability in nature, high stability, ease of fabrication, and low cost. Compounds derived from kesterite, such as Cu_2ZnSnS_4 (CZTS), $Cu_2ZnSnSe_4$ (CZTSe), and $Cu_2ZnSn(S,Se)_4$ (CZTSSe) have emerged as promising contenders for the cost-effective mass production of photovoltaic (PV) devices in the near future. It is worth mentioning that $Cu_2ZnSn(S,Se)_4$ (CZTSSe) is considered a chalcogenide material with a tunable band gap ranging from 1 to 1.5 electron volts and a significant absorption coefficient of 10^4 cm^{-1} [4]. Additionally, the conversion efficiency of CZTSe-based photovoltaic

* Corresponding author at: Departamento de Física, FACI, Universidad de Tarapacá, Casilla 7D, Arica, Chile.
E-mail addresses: lperez@academicos.uta.cl (L.M. Pérez), e.feddi@um5r.ac.ma (E. Feddi).

https://doi.org/10.1016/j.solener.2023.111929
Received 16 March 2023; Received in revised form 15 July 2023; Accepted 1 August 2023
Available online 23 August 2023

cells can reach almost 14.1% [5], which is lower than that of CIGSe thin film photovoltaic cells with a conversion efficiency of 20% [6]. In recent study, Kuldeep Singh Gour et al. [7] give an overview of the advancements in the CZTSSe-based kesterite thin films in terms of synthesis, material properties, and their use in various applications. In this interesting review the authors develop a comprehensive analysis of each device application contains ongoing progress, device fabrication, and related problems. In relation with the exploration of these materials, interesting reviews [8,9] have summarized and discussed in detail the state-of-art describing the problems related the CZTSSe solar cells. The authors suggested some strategies to enhance the power conversion efficiency with focus given to three critical device regions: kesterite absorber, buffer/kesterite interface, and kesterite/back contact interface. In order to understand the impact of defects, defect clusters and band tailing on the performance of $Cu_2ZnSn\ (S,Se)_4$ solar cells, V. C. Karade et al. [10] have proposed a detailed investigation leading to some important conclusions. The authors have shown that the relative concentration of the ZnCu and SnCu defects and B-type $[2Zn_{Cu} + Zn_{Sn}]$ and C-type $[2Cu_{Zn} + Sn_{Zn}]$ defect clusters plays an important role in the solar cell parameters (V_{OC}, fill factor (FF), and power conversion efficiency (PCE). In addition they have observed that the trend in short circuit current densities (J_{SC}) is independent of defects and defect cluster concentrations and the band tailing behavior can be affected by the existence of minor secondary phases on the kesterite surface. Strictly speaking, the microscopic carrier loss mechanisms and their impact on $Cu_2ZnSnSe_4$ (CZTSe) performance remain largely unknown. These mechanisms are investigated in recent study developed by Jianjun Li et al. [11] considering multiple microscopic and macroscopic characterizations with three-dimensional device simulations. Their conclusions indicate that CZTSe films have a relatively long intragrain electron lifetime of 10–30 ns and small recombination losses through bandgap and/or electrostatic potential fluctuations. They have shown that the effective minority carrier lifetime of CZTSe is dominated by a large grain boundary recombination velocity ($\sim 10^4$ cm s^{-1}), which is the major limiting factor of present device performance. On the other hand, the reduced power conversion performance of kesterite-based thin film solar cells can be also attributed to other effects such as the presence of secondary phases in ZnS, SnS, SnS_2, and Cu_2S, as well as unpredictable disorder and extensive CuZn and ZnCu antisite defects [12]. To mitigate these effects, one potential solution involves substituting alternate chemical elements with comparable valence configurations for Cu^+, Zn^{2+}, and Sn^{4+} ions. Replacing tin atoms with germanium atoms can increase the material's optical band gap, which represents the energy range required to excite electrons [13]. This substitution enables the material to be used alongside a photovoltaic cell with a low energy bandgap, facilitating the efficient conversion of a substantial portion of solar radiation into electrical energy while reducing defects associated with tin (Sn). CZGX (X=S or Se), specifically Cu_2ZnGeX_4, is a type of chalcogenide semiconductor that offers a tunable bandgap ranging from 1.3 to 2 electron volts [13]. However, substituting zinc with nickel in CZGS yields the compound Cu_2NiGeS_4 (CNGS), which has received less attention in solar cell research [14]. Researchers have conducted limited experimental investigations on these materials and have concluded that CNGS can be synthesized using a straightforward and costeffective method. They have also observed its high absorption rate and a bandgap of 1.8 eV [15]. Given these promising characteristics, CNGS emerges as a suitable candidate for solar cell applications, holding significant potential in this field. However, research on CNGS material is still in its early stage. Also, no such computational simulation carried out on CNGS to evaluate its photovoltaic properties. Such modeling could provide valuable insights and save time and resources before moving towards experimental cell fabrication. In our study, we carried out simulations to examine how various parameters affect the performance of CNGS solar cells. The parameters investigated included doping concentration, defect density, absorption layer thickness, buffer layer thickness, and window layer thickness. Moreover, we explored the use of suitable buffer layers such as CdS, ZnS, and their alloy $Cd_{1-x}Zn_xS$, each with different thicknesses, to improve the overall performance of the CNGS solar cell. Our primary goal was to maximize the photovoltaic parameters of the CNGS top cell, which encompassed J_{SC}, V_{OC}, FF, and efficiency. To achieve this objective, we utilized the SCAPS 1D simulator for conducting simulations. These simulations enabled us to identify the optimal values for the parameters, enhancing the overall performance of the CNGS solar cell.

2. DFT calculations

The first principle calculation is carried out using the density functional theory (DFT) with the help of Wien2k to obtain the electronic and optical characteristics of the CNGS material [16]. Here, the full-potential linearized augmented plan-wave (FP-LAPW) approach is utilized along with the Tran–Blaha modified Becke–Johnson potential, combined with the Hubbard potential of 0.44 Ry for correlation effects [17]. To ensure the accuracy of the obtained results, a convergence test is conducted with a product of Rmt and Kmax set to 9, 1000 k-points in the first Brillouin zone and a cut-off energy of −6 Ry. When the energy variation between two iterations is less than 10^{-4}, it is considered that the self-consistent calculation has converged [18].

The electronic structure of the kesterite CNGS material is crucial in determining its characteristics and selecting an appropriate exchange–correlation function for its modeling. The LDA and GGA method is generally used to calculate the band gap. However, it tends to inaccurately calculate the band gap energy in CNGS's electronic band structure [16].

To address this issue, a more suitable mBJ + U method is used to obtain a more accurate calculation of the band structure of CNGS, as shown in Fig. 1.a along the high symmetry directions. This approach offers a feasible solution and provides an accurate quantitative representation of CNGS. From Fig. 1.a, it is found that the peak of the valence band and the bottom of the conduction band are both located at the gamma point in the center of the Brillouin zone, indicating that CNGS is a direct bandgap semiconductor material [19]. The band gap energy was found to be 1.78 eV, which is approximately equal to the experimental result of 1.8 eV reported in the literature [15]. Additional detail about the electronic properties discussed in this paragraph can be found in Ref. [19]. The absorption coefficient of CNGS as a function of the incoming photons energy is presented in Fig. 1.b. Distinctly, CNGS displays a high absorption rate in the visible spectrum, with a coefficient of 10^4 cm^{-1}. Therefore, the CNGS can absorb light in the visible range with high efficiency, allowing it to be used for applications such as solar cells and photodetectors.

3. Simulation and material characterization of photovoltaic devices

SCAP-1D, equipped with sophisticated mathematical and physical models, is utilized here for the numerical modeling and simulation of the solar cell. It not only saves time but also the cost of development. The priority of numerical tools is providing solutions to real-time issues in a virtual platform. So, most design engineers and researchers from academia, and industry, go for simulation before the real-time fabrication of any device [20]. It provides details regarding different phenomena inside the device by considering material physical properties and mathematical models. In this modeling, the material's physical properties were used as inputs for simulation software. These properties are listed in Table 1. The simulation software solves fundamental semiconductor physics equations, including the continuity equation for both electrons and holes and the Poisson equation, which relates the charge to the electrostatic potential [21,22].

$$\frac{\partial^2 \Psi(x)}{\partial x^2} = \frac{-q}{\varepsilon_s}\left[N_D^+ - N_A^- + P(x) - n(x) + \rho(n,p)\right] \quad (1)$$

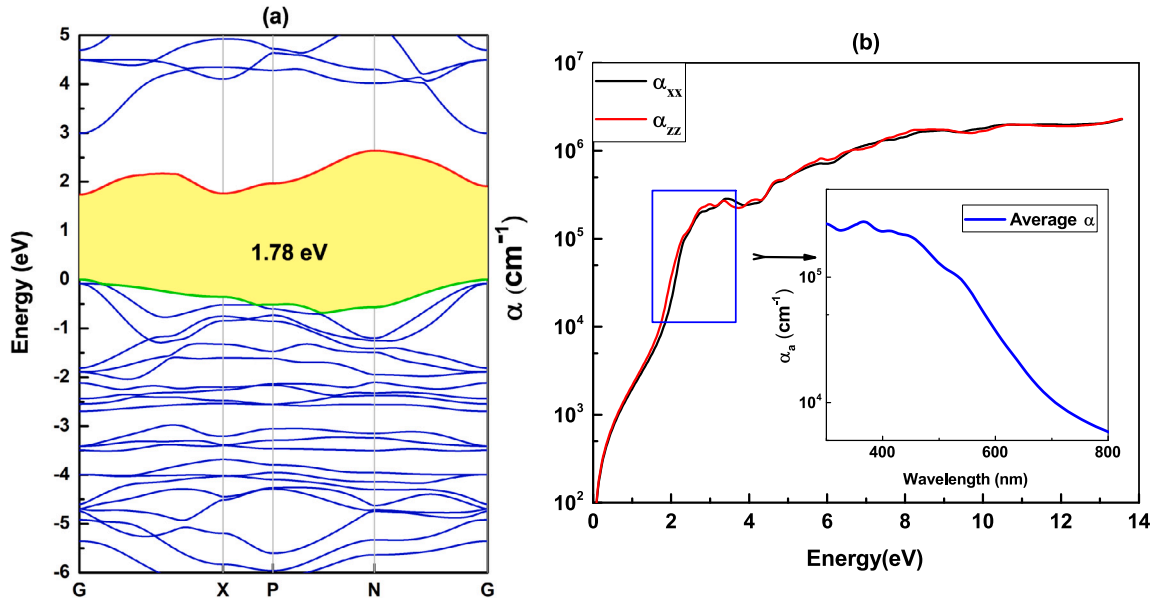

Fig. 1. The band structure of CNGS along the high symmetry directions (a) and the CNGS absorption coefficient spectra as a function of the energy of the incident photons (b).

where Ψ represents electrostatic potential, q represents elementary electrical charge, ϵ_s represents static relative permittivity, p and n represent hole and electron density, N_D^+ and N_A^- represent ionized donor and acceptor density, and $\rho(n,p)$ is the charge located in deep states. Additionally, the electron and hole current density can be calculated by using the following formula:

$$\frac{\partial n}{\partial t} = \frac{1}{q}\frac{\partial J_n}{\partial x} + G - R\ ,\ \frac{\partial p}{\partial t} = -\frac{1}{q}\frac{\partial J_p}{\partial x} + G - R \tag{2}$$

The current densities of electrons and holes are denoted by j_n and j_p, respectively. The recombination rate is represented by R, while the generation rate is denoted by G. The transport of charge carriers in semiconductors through the drift and diffusion process is expressed as follows:

$$J_n = q\mu_n nE + qD_n\frac{dn}{dx}\ ,\ J_p = q\mu_p pE - qD_p\frac{dp}{dx} \tag{3}$$

where $\mu_{(n,p)}$ is electron and hole mobility, $D_{(n,p)}$ is diffusion coefficient of electrons and holes. The modeling tool calculates the physical parameters such as hole and electron concentration, electrical potential, J–V characteristics of the device and functional parameters like conversion efficiency, fill factor and open circuit voltage.

The design of CZTS and CIGS solar cells served as the basis for CNGS, which forms a kesterite structure when used as thin films [23]. The proposed device was built on a glass substrate as the back support and a molybdenum layer was deposited on it. A 40–200 nm thick MoS_2 (p-type) layer was added, followed by a 400–2400 nm thick CNGS (p-type) absorber layer and a 20–100 nm thick CdS (n-type) buffer layer to form the PN junction. An 80 nm thick intrinsic ZnO (n-type) layer and a 200 nm thick Al-doped ZnO (ZnO:Al) layer were used as the transparent conducting oxide layer, acting as the window layer of the solar cell. The layer arrangement is illustrated in Fig. 2.

The accurate solution of the semiconductor equations reveals the correct behavior of the device, and it requires a thorough understanding of the material's physical properties. This study requires the physical parameters to be obtained from various sources such as experimental studies, literature, and DFT calculations.

Table 1 provides a comprehensive compilation of the input parameters utilized in the numerical analysis conducted with the SCAPS 1D software. Table 2, on the other hand, outlines the specific characteristics of the front and back contact parameters [23]. The absorber layer in the simulation considers only one type of defect located at the center of the band gap, having a capture cross-section of 10^{-14} cm^2 for both

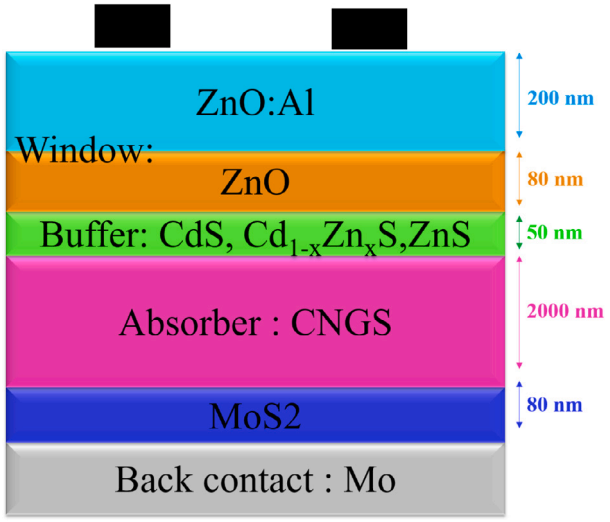

Fig. 2. Structure of CNGS based solar cells.

electrons and holes and a density of 10^{15} cm^{-3} [24]. The simulation used absorption coefficient data for each layer, obtained from external sources. The data for the CNGS layer was obtained from Fig. 1.b, while the data for the other layers were obtained from experimental results found in the literature [19].

In this study, we have considered the experimental series and shunt resistances of CZTS as 4.5Ω cm^2 and 340 Ω cm^2, respectively [19]. The simulations were carried out using AM 1.5 G solar radiation with a power density of 100 mW/cm^2. To optimize the performance of the photovoltaic device, the J–V curve, band alignment diagram, spectral response, and other important parameters, such as open-circuit voltage (V_{OC}), short-circuit current density (J_{SC}), and fill factor (FF), are analyzed [25]. These parameters are crucial for determining the efficiency of the solar cell and are essential for the optimization process.

Table 1
The physical parameters of each layer were used to simulate a CNGS solar cell at T = 300 K [19,23,26,27].

Parameters	ZnO:Al	ZnO	CdS	CNGS	MoS_2
Thickness (nm)	200	80	50	2000	80
Bandgap (eV)	3.3	3.3	2.4	1.8	1.3
Electron affinity (eV)	4.5	4.5	4.4	4.3	4.2
Dielectric permittivity	9	9	10	6.56	4
CB effective density of states (cm^{-3})	2.2 10^{18}	2.2 10^{18}	2.2 10^{18}	2.58 10^{18}	7.5 10^{17}
VB effective density of states (cm^{-3})	1.8 10^{19}	1.8 10^{19}	1.8 10^{19}	4.54 10^{18}	1.8 10^{18}
Electron thermal velocity (cm/s)	10^7	10^7	10^7	10^7	10^5
Hole thermal velocity (cm/s)	10^7	10^7	10^7	10^7	10^7
Electron mobility (cm^2/Vs)	100	100	100	100	100
Hole mobility (cm^2/Vs)	25	25	25	25	150
Shallow uniform donor density N_D (cm^{-3})	10^{18}	10^{18}	10^{18}	0	0
Shallow uniform acceptor density N_A (cm^{-3})	0	0	0	10^{16}	10^{15}
Absorption	Scaps file	Scaps file	Scaps file	Data Fig. 1.b	Experimental data [28]

Table 2
Back and front contact parameters properties at T = 300 K [23].

Parameters	Left contact(back)	Right contact (Front)
Surface recombination velocity of electrons (cm/s)	1 × 10^5	1 × 10^7
Surface recombination velocity of holes (cm/s)	1 × 10^7	1 × 10^7
Work function (ev)	5	4.42

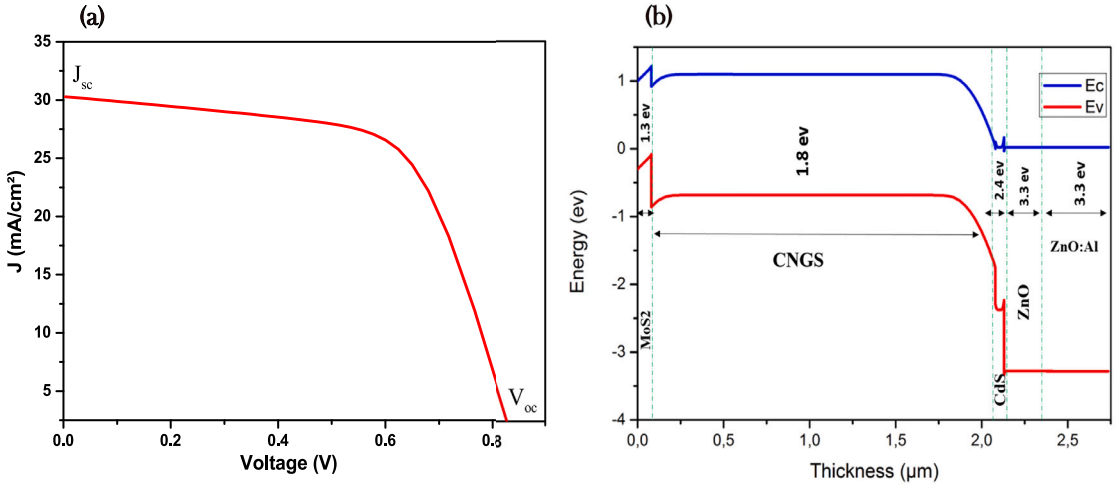

Fig. 3. (a) Performance analysis of CNGS solar cell using J–V plot. (b) The CNGS solar cell device's energy band diagram.

4. Results and discussion

4.1. The basic design of device

Using the SCAPS-1D, the Mo/MoS_2/CNGS/CdS/ZnO/ZnO:Al device was analyzed. Fig. 3.a displays the current density versus voltage curve, revealing an efficiency of 16.08%, an open circuit voltage of 0.844 V, a short circuit current of 30.30 mA/cm^2, and a fill factor of 62.83%. However, this device's low open circuit voltage (Voc) may be due to bulk defects that could act as recombination centers for photo-generated carriers. The band diagram for the CNGS baseline cell is presented in Fig. 3.b. The spike-like structure at the interface of the CNGS absorber layer and the CdS buffer layer reduces the recombination rate and improves the collection of photo-generated electrons, leading to a higher J_{sc} and a more efficient solar cell [29]. Therefore, optimizing the device structure and reducing the presence of bulk defects could lead to further improvements in the performance.

4.2. Impact of layers thickness on device efficiency

Fig. 4 shows the effect of CNGS absorber layer thickness on solar cell performance. The absorber layer thickness is varied between 400 to 2400 nm, and the outcomes are illustrated in Fig. 4. A slight increase in open-circuit voltage was observed. It is due to the increment in thickness of the absorber layer, which results in an increment in majority charge carriers. However, there was a significant increase in J_{sc} as the thickness of the absorber increased, as revealed in Fig. 4. This change was due to increased photogenerated charge carriers in thicker absorber layers, resulting in improved efficiency. It is also observed that increasing the thickness of the absorber caused a minimal change in FF, which ranged from 60% to 63% over the entire thickness range. The variation in fill factor is likely linked to resistive losses [30].

The wavelength of light and its effect on the generation of electron–hole pairs can be studied from the quantum efficiency (QE) curve. These variations are caused by the thickness of the CNGS layer, as a thicker CNGS layer can absorb more photons across a broader wavelength range [31]. Fig. 5 depicts how CNGS thickness affects QE%. The QE% improved as the thickness of the CNGS layer increased. As the thickness of the CNGS absorber layer increases, there is an increase in the amount of material available to absorb incident light. This increase in material provides more opportunities for photons to interact with the absorbing layer and generate electron–hole pairs. As a result, the amount of light absorbed by the solar cell increases. Greater light absorption leads to an increase in photocurrent, the electric current generated by the solar cell when it is exposed to light. The more photons absorbed, the more electron–hole pairs generated and the

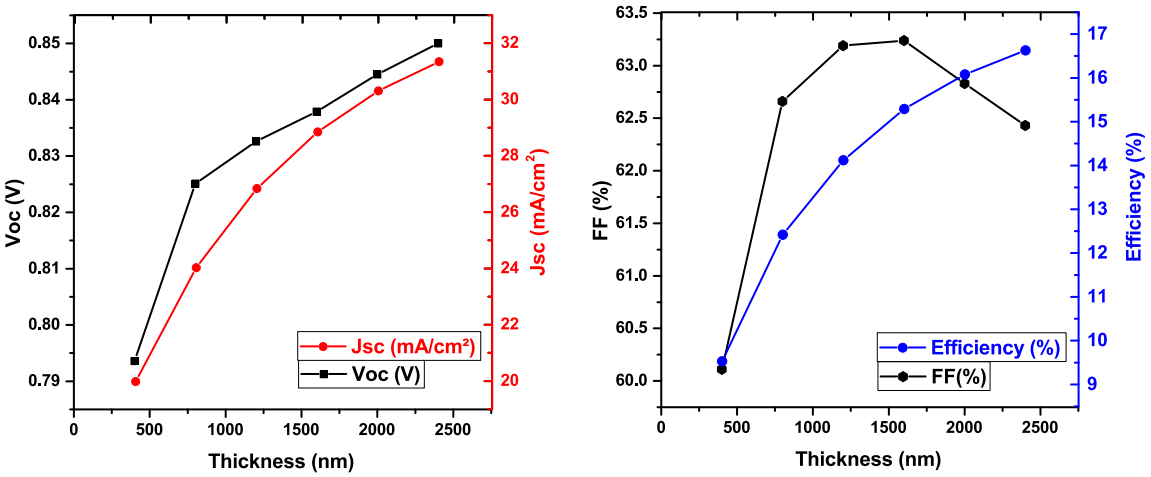

Fig. 4. The effect of CNGS layer thickness on the V_{oc}, J_{sc}, FF and efficiency of the cell.

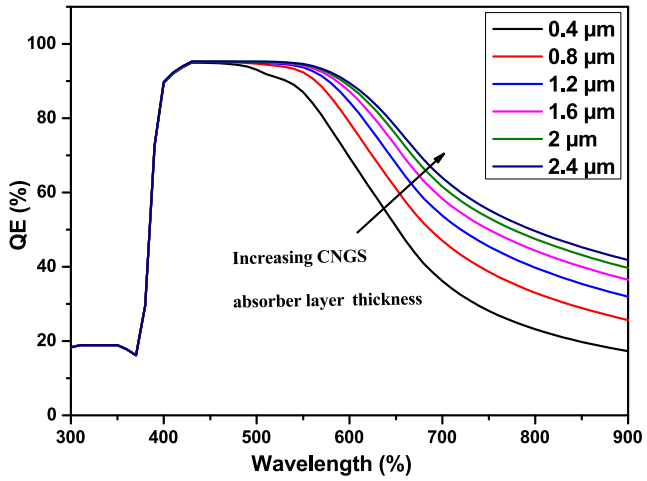

Fig. 5. Quantum efficiency percentage (QE%) for the cell at different thicknesses. Layer thicknesses of MoS_2, CdS, ZnO, and ZnO:Al of 80 nm, 50 nm,80 nm, and 200 nm respectively, were assumed for calculations under T = 300 K.

higher the photocurrent. Since cell current increases considerably as CNGS layer thickness increases up to 2400 nm, the QE spectrum also magnifies in this range. The layer thickness of more than 2000 nm has little significant effect on the pace of QE% increases due to incoming light absorption saturation. This increase in photocurrent can contribute to an increase in the overall efficiency of the solar cell, as it indicates that more light energy is being converted into electricity. The results suggest that 2400 nm thickness is sufficient for absorbing most incoming photons, as this thickness results in the highest conversion efficiency of 16.63% as illustrated in Fig. 4.

MoS_2 has recently gained significant attention due to its distinctive electronic properties, which include high optical transparency, excellent carrier transport capabilities, and remarkable chemical, mechanical, and thermal stability [32]. The interface between Molybdenum and CNGS has been observed to have a mismatch, leading to an increase in series resistance (R_s) and consequently, recombination. This has a negative effect on the V_{oc} (open-circuit voltage) [19]. However, the inclusion of a thin layer of molybdenum disulfide (p-MoS_2), the back surface field (BSF), can effectively reduce the recombination rate. By creating an integrated electric field on the back surface, the p-MoS_2 layer acts as a barrier, preventing electrons and holes from recombining between the absorber layer and the molybdenum back contact. As a result, the Voc of the solar cell can be improved [32].

The impact of carrier transport layer (MoS_2) thickness on solar cell performance is demonstrated in Fig. 6. Adding a p-MoS_2 layer at the interface of the absorber layer and the metal contact resulted in a slight modification in the solar cell characteristics, with an improved efficiency resulting in V_{oc} = 0.849 V, J_{sc} = 30.30 mA/cm^2, and FF = 62.90%, with η = 16.20%. The highest efficiency of 16.20% was achieved for a 200 nm film. by augmenting the thickness of the MoS_2 layer, more conductive paths for charge carriers, allowing electrons or holes to move through the material more easily. This results in reduced resistance and increasing the thickness of the carrier transport layer leads to smoother transport of photogenerated holes in the solar cell. As can be seen, all parameters undergo minor changes only when they exceed 100 nm, which indicates that this thickness may be sufficient to achieve good performance.

The simulation goal is to minimize the optical and electrical radiation losses from the buffer layer resulting from exposure to solar radiation. Fig. 7 depicts the simulation results for a CdS layer with a thickness range of 20 nm to 100 nm. The findings show that increasing the CdS layer thickness had a limited impact on the solar device performance, particularly on open-circuit voltage, fill factor, and efficiency conversion rate, and only had a slight impact on short-circuit current density [33]. The reason for the minimal impact on short-circuits current and fill factor is that a thicker CdS layer causes photon losses. The thicker buffer layer absorbs more photons from the incoming radiation, reducing the QE% and the number of photons reaching the CNGS layer for absorption, resulting in fewer photogenerated electron–hole pairs [34]. Conversely, a thinner buffer layer leads to leakage current, while a thicker one causes a low carrier separation rate. Based on these findings, it is recommended that the buffer layer thickness be set to 50 nm for optimal performance.

4.3. The influence of the defect density effect of the CNGS absorber

Effective generation and recombination within the absorber layer are the most crucial parameters for attaining optimal efficiency. Recombination in the absorber layer is triggered by defect density. Therefore, comprehending the impact of defect densities on device performance is imperative to achieve a maximum yield. The defect density in the CNGS absorber is primarily composed of point defects, such as vacancy and interstitial. Defect density was varied between 10^{10} cm^{-3} and 10^{16} cm^{-3} to investigate the impact of defect density. Fig. 8 describes the evolution of the photovoltaic parameters according to the defect density. As illustrated in Fig. 8, the cell's performance remains reasonably stable when the defect density is lower than 10^{14} cm^{-3}. However, the output parameters are substantially affected when the defect density surpasses this threshold. It has been discovered that higher levels of defects in

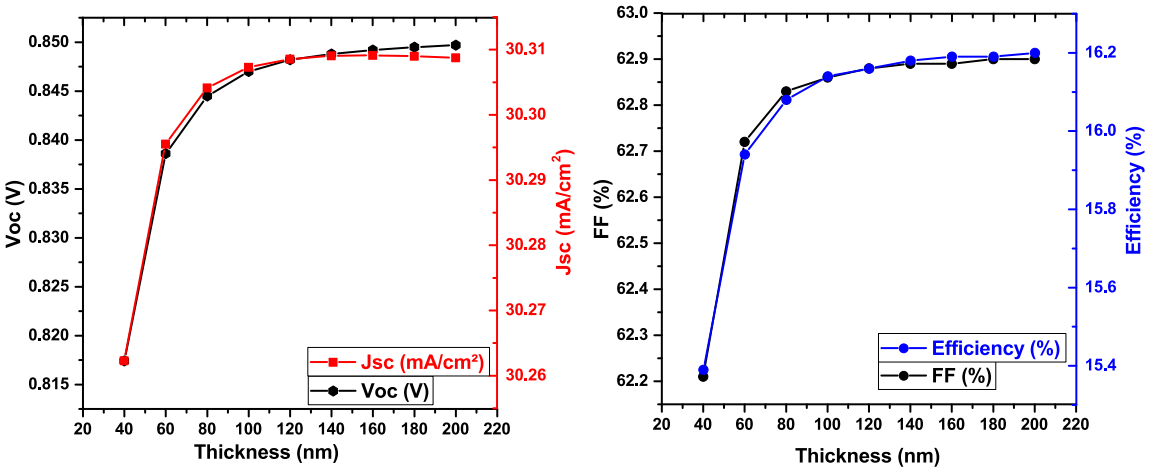

Fig. 6. The impact of MoS_2 layer thickness on V_{oc}, J_{sc}, FF and efficiency of CNGS solar cell.

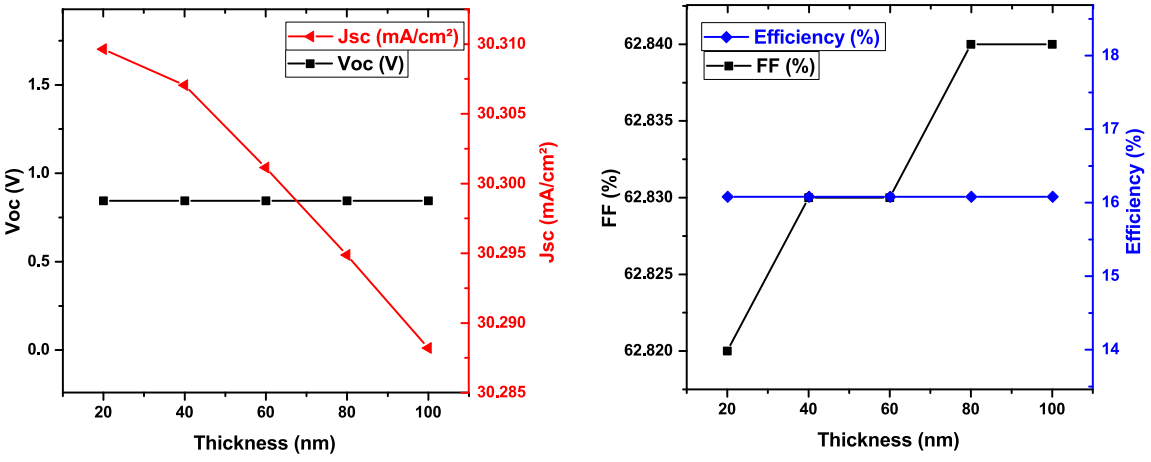

Fig. 7. Influence of the CdS buffer layer thickness on the J_{sc}, V_{oc}, FF and efficiency of solar cells at 300 K. The layer thicknesses of CNGS, MoS_2, ZnO, and ZnO:Al were kept constant at 2000 nm, 80 nm, 80 nm, and 200 nm, respectively.

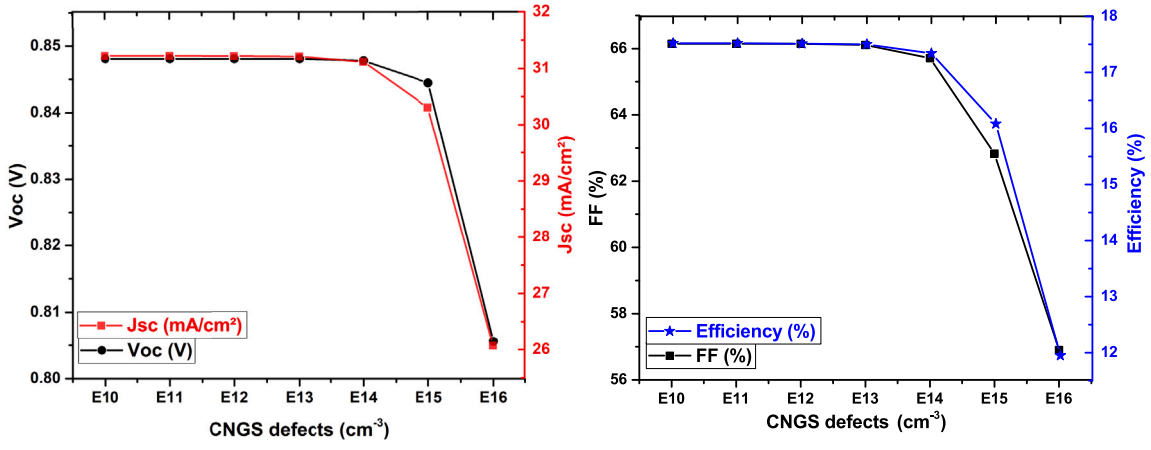

Fig. 8. The impact of defect density on the optoelectronic properties of CNGS solar cell.

the CNGS absorption layer lead to significant recombination and film deterioration, culminating in reduced stability and overall performance of the cell [23]. This suggests that an increase in the defect states in the absorber layer creates more recombination centers, resulting in more robust recombination of photo-generated carriers, ultimately decreasing J_{sc}, V_{oc}, conversion efficiency, and fill factor.

4.4. The effect of doping concentration on device behavior

Fig. 9 demonstrates the impact of varying the acceptor carrier concentration (N_A) of the CNGS absorber layer from 10^{10} cm^{-3} to 10^{18} cm^{-3} on the cell characteristics. The figure shows that the J_{sc} decreases as the absorber doping increases, whereas V_{oc} increases. These phenomena

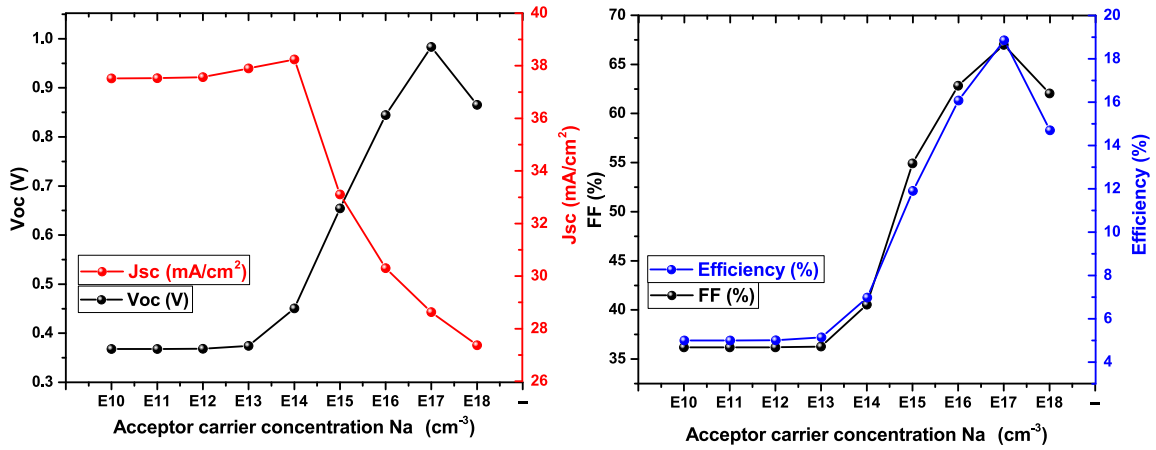

Fig. 9. The impact of absorber carrier concentration (N_A) on the cell efficiency parameter (T = 300 K) in the CNGS material.

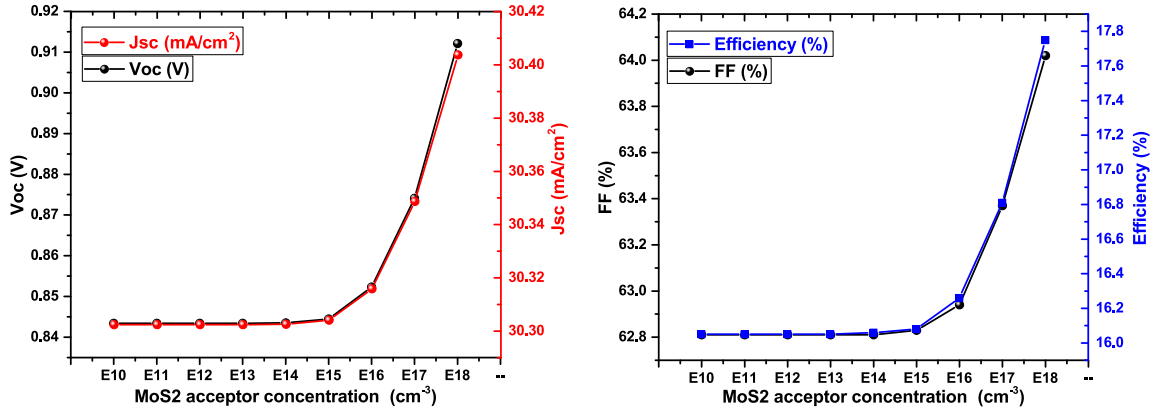

Fig. 10. The effect of MoS_2 carrier concentration (N_A) on cell optoelectronic parameters.

can be elucidated by the Shockley equation in the context of a simple p–n junction model [35].

$$I_0 = Aqn_i^2\left(\frac{D_e}{L_eN_A}+\frac{D_h}{L_nN_D}\right)$$
$$V_{oc} = \frac{KT}{q}ln\left(\frac{I_L}{I_o}+1\right) \quad (4)$$

The saturation current decreases as the carrier density increases, resulting in a higher open-circuit voltage. However, the short-circuit current decreases due to the increased recombination process and reduced quantum efficiency of longer wavelength photons. The fill factor initially increases as the carrier density increases from 10^{14} to 10^{17} cm^{-3}, but then decreases beyond this point due to enhanced mobility and reduced carrier lifetime . At high carrier densities, the mobility of the charge carriers increases due to the stronger electric fields, leading to increased recombination and a decrease in the useful carrier lifetime, thus causing a decline in the FF. The energy conversion efficiency of the solar cell begins to decline when the carrier density exceeds 10^{17} cm^{-3} due to the increased recombination of carriers. A carrier density of 10^{17} cm^{-3} achieved the highest energy conversion efficiency of 18.86%.

Fig. 10 presents the impact of adjusting the carrier concentration of the interlayer MoS_2 from 10^{10} cm^{-3} to 10^{18} cm^{-3} on the cell parameters is presented. Including of the MoS_2 layer as a back surface field reduces the recombination rates, creating a built-in electric field that acts as a barrier to prevent the recombination of electrons and holes. Increasing the carrier acceptor concentration in MoS_2 results in fewer recombination centers, a lower recombination rate, and improved cell efficiency in the CNGS solar cell. In addition, an increase in carrier concentration leads to a decrease in the Fermi level (E_F), which in turn reduces carrier recombination [32]. At an acceptor concentration of 10^{18} cm^{-3} in MoS_2, the cell attains an efficiency of 17.75%, with a V_{oc} of 0.912 V, a J_{sc} of 30.40 mA/cm^2, and an FF of 64.02%.

The carrier concentration level of the CdS layer was changed from 10^{10} to 10^{18} cm^{-3} to accomplish this. The CdS buffer impact on the CNGS performance characteristics is depicted in Fig. 11. The obtained results suggest that there are no changes in V_{oc}, J_{sc}, FF and efficiency up to the doping concentration (N_D) of 10^{15} cm^{-3} of buffer layer. A further increase in the doping level has resulted in an overall CNGS efficiency improvement at a higher donor concentration of 10^{18} cm^{-3}. However, keeping the buffer layer as thin as possible with a very high doping level to maintain the remarkable overall CNGS-based solar cells performance.

4.5. Effect of different buffer layers on cell performance

The buffer layer plays a pivotal role in generating the electric field within the space charge region at the junction. The objective of this investigation is to examine the impact of different buffer layers, specifically CdS, ZnS, and their $Cd_{1-x}Zn_xS$ alloy, on the efficiency of the CNGS photovoltaic cell. To evaluate the influence of the buffer layer, its thickness was varied within the range of 20 to 100 nm, while the CNGS layer thickness was kept constant at 2000 nm. Additionally, a single acceptor-type defect with a defect density of 10^{15} cm^{-3} was introduced

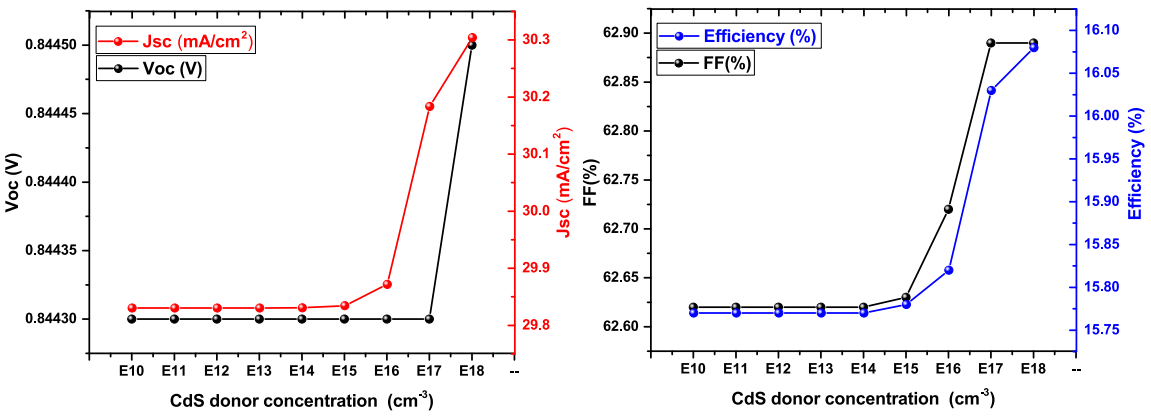

Fig. 11. Illustrates the impact of carrier concentration (N_D) in the buffer layer (CdS) on the cell efficiency parameter.

Table 3
The electric parameters for electron transport layers of $Cd_{1-x}Zn_xS$ are employed in this simulation, where x represents the molar concentration of Zn [36–38].

Parameters	x = 0.2	x = 0.3	x = 0.5	x = 1
Thickness (nm)	20–100	20–100	20–100	20-100
E_g (eV)	2.58	2.64	2.7	3.5
X (eV)	4.38	4.32	4.26	4.5
ϵ	9.3	9.3	9.3	10
N_c (cm^{-3})	2.1 10^{18}	2.1 10^{18}	2.1 10^{18}	1.8 10^{18}
N_v (cm^{-3})	1.7 10^{19}	1.7 10^{19}	1.7 10^{19}	1.8 10^{19}
v_e (cm/s)	10^7	10^7	10^7	10^7
v_h (cm/s)	10^7	10^7	10^7	10^7
μ_e (cm^2/Vs)	85	75	70	100
μ_h (cm^2/Vs)	30	25	20	25
N_D (cm^{-3})	10^{18}	10^{18}	10^{18}	10^{18}
N_A (cm^{-3})	0	0	0	0
Absorption	Scaps file	Data	Data	Scaps file

in the buffer layer. The input parameters for the different buffer layers are presented in Table 3.

Fig. 12 illustrates the changes in solar cell parameters such as open-circuit voltage (V_{oc}), short-circuit current density (J_{sc}), fill factor (FF), and efficiency (η) as the buffer layer thickness increases. The buffer layers of CdS, $Cd_{0.8}Zn_{0.2}S$, $Cd_{0.7}Zn_{0.3}S$, and $Cd_{0.5}Zn_{0.5}S$ exhibit comparable characteristics due to their close band gap energies, leading to similar performance outcomes. The similarity in band gap energies results in comparable absorption characteristics and electron–hole pair generation in the absorber layer [34]. However, The bandgap of the ZnS buffer layer is relatively higher than that of the other buffer layers, it is important to highlight that its performance deviated from the others in terms of J_{sc} and overall efficiency values. This deviation can be attributed to the distinct characteristics of the band diagram between ZnS and the other materials used. Unlike the other buffer layers, ZnS does not exhibit a spike-shaped interface. This absence of a spike-shaped interface in ZnS leads to a different energy band alignment compared to the other buffer layers. Consequently, the mechanisms governing charge separation and transport may vary in the ZnS-based configuration. These discrepancies in band alignment and interface structure between ZnS and the other materials likely contribute to the observed differences in J_{sc} and efficiency values. The presence of a spike-shaped interface, as seen in the CNGS/CdS configuration, creates a favorable energy band alignment. Specifically, the conduction band of the absorber material (CNGS) is higher than the conduction band of the buffer layer material (CdS). This energy level offset facilitates efficient separation of the photogenerated electrons from the absorber layer, as they can readily migrate to the conduction band of the buffer layer. In the absence of the spike-shaped interface, such as in the CNGS/ZnS configuration, the band alignment is different. The energy levels of the conduction bands in CNGS and ZnS may be more closely aligned. As a result of this less favorable band alignment, the charge extraction process becomes less efficient. In this configuration, a lower built-in voltage is observed for ZnS. This could explain why, despite the expected higher photon absorption in ZnS, a slightly lower value of J_{sc} is obtained, since the electric field is weakened in comparison to the device with CdS to separate the photogenerated electron–hole pairs. Additionally, the presence of a higher concentration of zinc (Zn) in the band diagram creates complexities in the movement of charged carriers, affecting carrier transport. This complication lead to similar behavior in the short-circuit current and open-circuit voltage. In the case of fill factor (FF) shows an slight increasing trend in the ZnS buffer layer, while no significant change is observed in the fill factor for CdS and other buffer layers. Fig. 12d depicts the efficiency curves for the different buffer layers. The results indicate that the efficiency of the solar cell featuring ZnS buffer layers is slightly lower by over 0.5% compared to CdS, and this trend exhibits a slight decline with an increase in thickness. In contrast, it can be observed that the efficiencies of CdS and other buffer layers display a slight increase. The fluctuations in efficiency are influenced by the combined effects of V_{oc}, J_{sc}, and fill factor. The ZnS buffer layer shows a higher rate of decline in J_{sc}, leading to a decrease in efficiency. The findings indicate that the efficiency of buffer layers consisting of $Cd_{0.8}Zn_{0.2}S$ and $Cd_{0.5}Zn_{0.5}S$ increases slightly with the increase in thickness as it exhibited excellent efficiencies of 16.13% and 16.12%, respectively. Therefore, the study proposes $Cd_{0.8}Zn_{0.2}$ and $Cd_{0.5}Zn_{0.5}S$ as promising alternatives to CdS as a buffer layer. Table 4 summarizes the optimal efficiencies for CdS, ZnS, and their alloys based on the obtained results.

5. Best device performance

In our study, our primary aim was to identify the most effective combinations of parameters to enhance the efficiency and stability of CNGS-based solar cells. Here, we present a summary of the optimized parameters and simulation outcomes. The outcomes indicate that a thickness of 2400 nm for the absorber layer in CNGS solar cells is the most suitable. The highest energy conversion efficiency is attained with a carrier density of 10^{17} cm^{-3}. For MoS_2, the optimal thickness is 100 nm, and the highest efficiency is achieved with an acceptor concentration of 10^{18} cm^{-3}. The simulations also demonstrate that utilizing a 50 nm thick buffer layer composed of $Cd_{0.8}Zn_{0.2}S$ leads to exceptional efficiency. However, it is preferable to keep the buffer layer as thin as possible with a highly doped configuration, necessitating a carrier donor concentration of 10^{18} cm^{-3}. The optimized outcomes yield an efficiency conversion rate of 20.05%, a fill factor of 66.77%, a short-circuit current of 29.67 mA/cm^2, and an open-circuit voltage of 0.983 V. In order to offer a thorough depiction of our numerical simulations, we have condensed our findings into a concise comparison presented in Table 5. Additionally, to enhance the depth of our study, we have

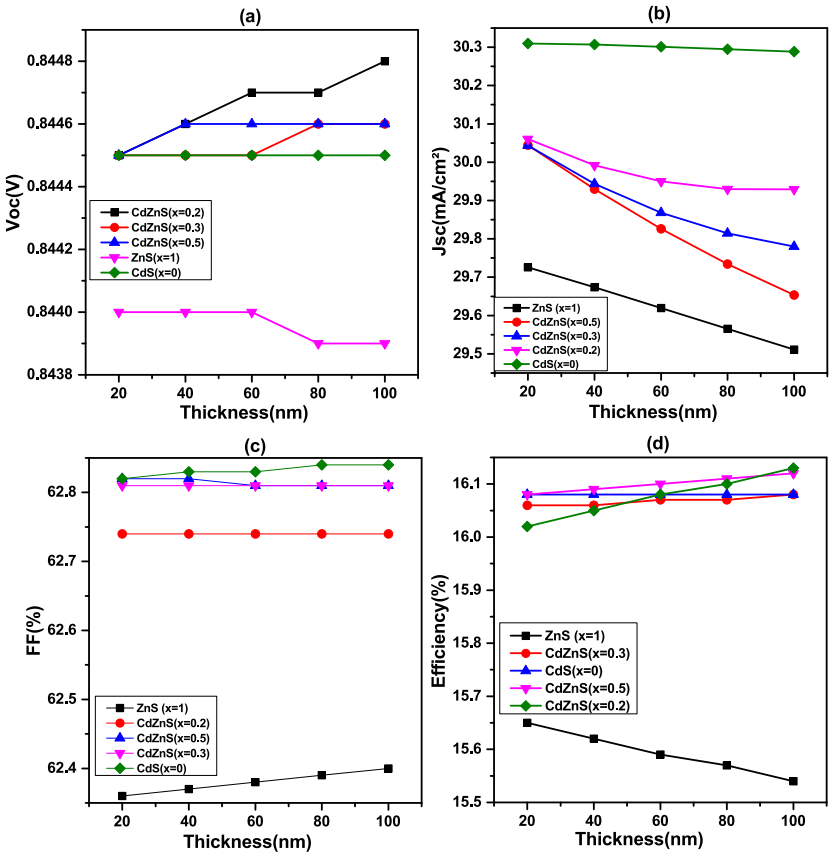

Fig. 12. Open-circuit voltage (a), short-circuit current density (b), Fill factor (c) and Efficiency (d) for different buffer layer thicknesses.

Table 4
Investigating the performance of CNGS solar cells through photovoltaic analysis.

Thin film solar cell	V_{oc} (V)	J_{sc} (mA/cm^2)	FF (%)	η (%)
Mo/MoS_2/CNGS/CdS/ZnO/ZnO:Al	0.8445	30.3070	62.83	16.08
Mo/MoS_2/CNGS/$Cd_{0.8}Zn_{0.2}S$/ZnO/ZnO:Al	0.8448	30.4278	62.74	16.13
Mo/MoS_2/CNGS/$Cd_{0.7}Zn_{0.3}S$/ZnO/ZnO:Al	0.8446	30.3126	62.81	16.08
Mo/MoS_2/CNGS/$Cd_{0.5}Zn_{0.5}S$/ZnO/ZnO:Al	0.8446	30.3868	62.81	16.12
Mo/MoS_2/CNGS/ZnS/ZnO/ZnO:Al	0.8439	29.5108	62.40	15.54

Table 5
A comparison table showcasing the optimal CNGS cell alongside other CZTS cells found in the literature.

Absorber layer	V_{oc} (V)	J_{sc} (mA/cm^2)	FF (%)	η (%)	References
CNGS	0.983	29.67	66.77	20.05	Present Study
CZTS	0.479	36.9	70.45	12.45	Experimental [11]
CZTS	0.744	32.585	75.43	18.29	Theoretical [40]
CZTS	0.99	21.89	69.79	15.23	Theoretical [41]

integrated valuable insights from various sources, paying special attention to CZTS-based solar cells [39]. Both CNGS and CZTS materials have demonstrated promising performance in the field of solar cell applications. Although the specific efficiency values may differ, our analysis reveals that CNGS exhibits comparable results to CZTS. This suggests that CNGS holds significant potential as a viable alternative to CZTS in the context of solar cell technology . These findings underscore the remarkable prospects for advancements in solar cell technology, especially within the domain of CNGS-based thin-film solar cells. By highlighting the performance and potential of CNGS.

6. Conclusion

This study utilized SCAPS tool to model and assess a Mo/MoS_2/Cu_2NiGeS_4 (CNGS)/CdS/ZnO/ZnO:Al based kesterite solar cell. This research highlights the importance of numerical modeling in solar cell development and emphasizes the need for accurate and reliable simulations to understand and optimize the performance of CNGS-based systems. Firstly, the band gap energy and absorption coefficient of CNGS was determined to be 1.78 eV and 10^4 cm^{-1} using the mBJ + U potential, indicating its potential as a promising material for photovoltaic devices. This study also investigated the impact of various parameters, such as layer thickness, donor and acceptor concentrations, and defects, on the performance of CNGS absorber layer. Suitable buffer layers such as CdS, ZnS, and $Cd_{1-x}Zn_xS$ were explored to improve overall performance. By optimizing these parameters, a significant improvement in efficiency was obtained, with a conversion rate of 20.05%, a fill factor of 66.77%, a short-circuit current of 29.67 mA/cm^2, and an open-circuit voltage of 0.983 V. Overall, the results show that the CNGS's has the potential as a promising material for photovoltaic devices.

Declaration of competing interest

The authors declare that they have no known competing financial interests or personal relationships that could have appeared to influence the work reported in this paper.

Acknowledgments

L.M.P. acknowledges financial support from ANID through Convocatoria Nacional Subvención a Instalación en la Academia Convocatoria Año 2021, Grant No. SA77210040.

References

[1] N. Mariotti, M. Bonomo, L. Fagiolari, N. Barbero, C. Gerbaldi, F. Bella, C. Barolo, Green Chem 22 (2020) 7168–7218.
[2] W. Obergassel, C. Arens, L. Hermwille, N. Kreibich, F. Mersmann, H.E. Ott, H. Wang-Helmreich, 2015.
[3] Tang Jiao Huang, Xuesong Yin, Guojun Qi, Hao Gong, Physica Status Solidi (RRL)–Rapid Res. Lett. 8 (2014) 735–762.
[4] P. Fan, Z. Xie, G. Liang, M. Ishaq, S. Chen, Z. Zheng, C. Yan, J. Huang, X. Hao, Y. Zhang, Z. Su, J. Energy Chem. 61 (2021) 186.
[5] Jiazheng Zhou, Xiao Xu, Huijue Wu, Jinlin Wang, Licheng Lou, Kang Yin, Yuancai Gong, Jiangjian Shi, Yanhong Luo, Dongmei Li, Hao Xin, Qingbo Meng, Nature Energy 8 (2023) 526–535.
[6] Jessica Eid, Haifan Liang, Issam Gereige, Sang Lee, Jeroen Van Duren, Prog. Photovolt: Res. Appl. 23 (2015) 269–280.
[7] Kuldeep Singh Gour, Vijay Karade, Pravin Babar, Jongsung Park, Dong Min Lee, Vidya Nand Singh, Jin Hyeok Kim, Solar RRL 5 (2021) 2000815.
[8] Ao Wang, Mingrui He, Martin A. Green, Kaiwen Sun, Xiaojing Hao, Adv. Energy Mater. 13 (2023) 2203046.
[9] Mingrui He, Chang Yan, Jianjun Li, Mahesh P. Suryawanshi, Jinhyeok Kim, Martin A. Green, Xiaojing Hao, Adv. Sci. 8 (2021) 2004313.
[10] Vijay C. Karade, Mahesh P. Suryawanshi, Jun Sung Jang, Kuldeep Singh Gour, Suyoung Jang, Jongsung Park, Jin Hyeok Kim, Seung Wook Shin, J. Mater. Chem 10 (2022) 8466.
[11] Jianjun Li, Jialiang Huang, Fajun Ma, Heng Sun, Jialin Cong, Karen Privat, Richard F. Webster, Soshan Cheong, Yin Yao, Robert Lee Chin, Xiaojie Yuan, Mingrui He, Kaiwen Sun, Hui Li, Yaohua Mai, Ziv Hameiri, Nicholas J. Ekins-Daukes, Richard D. Tilley, Thomas Unold, Martin A. Green, Xiaojing Hao, Nature Energy 7 (2022) 754, 764.
[12] J. Just, C.M. Sutter-Fella, D. Lützenkirchen-Hecht, R. Frahm, S. Schorr, T. Unold, Phys. Chem. Chem. Phys 18 (2016) 15988–15994.
[13] J. El Hamdaoui, M. El-Yadri, M. Farkous, M. Kria, M. Courel, M. Ojeda, L.M. Pérez, A. Tiutiunnyk, D. Laroze, E. Feddi, Nanomaterials 11 (2021) 2692.
[14] G.E. Delgado, V. Sagredo, Rev. Mex. Fis 237 (65) (2020) 510.
[15] M. Beraich, H. Shaili, E. Benhsina, Z. Hafidi, M. Taibi, F. Bentiss, A. Guenbour, A. Bellaouchou, A. Mzerd, A. Zarrouk, M. Fahoume, Appl. Surf. Sci. 527 (2020) 146800.
[16] J.P. Perdew, Int. J. Quantum Chem. 28 (497) (1985) 523.
[17] F. Tran, P. Blaha, Phys. Rev. Lett. 102 (2009) 226401.
[18] H.J. Monkhorst, J.D. Pack, Phys. Rev. B 13 (1976) 5188.
[19] J. El Hamdaoui, M. El-Yadri, K. Lakaal, M. Kria, M. Courel, M. Ojeda, L.M. Pérez, D. Laroze, E. Feddi, Sol. Energy 237 (2022).
[20] A. Niemegeers, S. Gillis, M. Burgleman, Proceedings of the 2nd World Conference on Photovoltaic Energy Conversion, 1998.
[21] Burgelman M., J. Verschraegen, S. Degrave, P. Nollet, Res. Appl. 12 (2004) 143–153.
[22] H. Movla, Optik 125 (2014) 67–70.
[23] L. Et-taya, T. Ouslimane, A. Benami, Sol. Energy 201 (2020) (2020).
[24] J. Li, Z. Yuan, S. Chen, X. Gong, S. Wei, Chem. Mater. 31 (826) (2019) 833.
[25] M. Burgelman, et al., SCAPS Manual, University of Gent, Belgium, 2018.
[26] S. Kukreti, G.K. Gupta, A. Dixit, Sol. Energy 225 (2021) 802–813.
[27] A.D. Adewoyin, M.A. Olopade, M.A. Chendo, Optik 133 (2017) 122–131.
[28] A.R. Beal, H.P Hughes, J. Phys. C: Solid State Phys. 12 (1979) 881.
[29] A. Haddout, A. Raidou, M. Fahoume, Appl. Phys. A 125 (2019).
[30] Samed Çetinkaya, Optik - Int. J. Light Electron Optics 181 (2019).
[31] Abd Elhalim Benzetta, Mahfoud Abderrezek, Mohammed Elamine Djeghlal, Optik 242 (2021).
[32] Haitian Luo a, Yi Zhang c, Hui Li, Sol. Energy 223 (2021).
[33] Samer H. Zyoud, Ahed H. Zyoud, Naser M. Ahmed, Anupama R. Prasad, Sohaib.Naseem Khan, Atef F.I. Abdelkader, Moyad Shahwan, Crystals 11 (2021).
[34] Farjana Akter Jhuma-Marshia Zaman Shaily, Mohammad Junaebur Rashid, Mater. Renew. Sustain. Energy 8 (2019).
[35] M. Djinkwi Wanda, S. Ouédraogo, F. Tchoffo, F. Zougmoré, J.M.B. Ndjaka, Int. J. Photoenergy (2016).
[36] S.V. Borse, S.D. Chavhan, Ramphal Sharma, J. Alloys Compd. 436 (2007).
[37] Xing Yu, Xiaoping Zou, Jin Cheng, Chuangchuang Chang, Zixiao Zhou, Guangdong Li, Baoyu Liu, Junqi Wang, Dan Chen, Yujun Yao, Mater. Res. Express 7 (2020).
[38] Farjana Akter Jhuma-Marshia Zaman Shaily Mohammad Junaebur Rashid, Mater. Renew. Sustain. Energy (2019).
[39] M. Ravindiran, C. Praveenkumar, Renew. Sustain. Energy Rev. 94 (2018).
[40] Samed Çetinkaya, Optik (2019).
[41] A.R. Latrous, R. Mahamdi, N. Touafek, M. Pasquinelli, Int. J. Thin. Fil. Sci. Tec 10 (2021).